Journal of Marine Research, 48, 793–823, 1990

Near-inertial and diurnal motions in the trajectories of mixed layer drifters

by Pierre-Marie Poulain[1,2]

ABSTRACT

We analyze the near-inertial/diurnal motions in the trajectories of surface mixed layer drifters in the California Current System between 19N and 36N. The observed near-inertial or diurnal oscillations are very intermittent in time and have a time scale of about 10 inertial periods. Using a simple slab model of wind-driven inertial currents, we show that their temporal variations are related to the fluctuations in the local wind stress field. Three events of strong (20 cm s^{-1}) near-inertial/diurnal motions are studied in detail. Two events at the diurnal frequency occur on the continental shelf. For the first, the observed subinertial oscillations are interpreted as continental shelf waves generated by the diurnal tide currents and the local winds. For the second, observations are consistent with wind-driven internal waves. A third event of near-inertial oscillations appears for most of the drifters in the wake of a tropical storm. The vorticity of the background mesoscale circulation shifts the frequency of the wind-generated oscillations by as much as ±0.05 cpd.

1. Introduction

High-frequency horizontal currents, such as inertial and tidal motions, represent a major component of the kinetic energy of the oceans. Inertial currents (also called inertial oscillations or waves) are characterized by anticyclonic rotation of horizontal current with frequency near the local inertial frequency f, defined as $2\,\Omega \sin \Psi$, where Ω is the rotational frequency of the earth and Ψ is the latitude. They have been observed in the oceans and large lakes at all depths (Webster, 1968) with velocities of 10–80 cm s^{-1}. They have a vertical coherence scale of a few tens of meters and a horizontal scale of a few tens to a few hundreds of kilometers. They are highly intermittent and typically last a few inertial periods. Inertial waves are the most energetic and lowest frequency constituent of the internal wave field. The observed frequency is generally slightly above f and the surface-generated near-inertial waves are characterized by an upward propagation of phase and a downward propagation of energy. The blue shift in frequency is related to the variation of f with latitude or the

1. Present address: Cooperative Institute of Marine and Atmospheric Studies, University of Miami, 4600 Rickenbacker Causeway, Miami, Florida, 33149, U.S.A.
2. Scripps Institution of Oceanography, La Jolla, California, 92093, U.S.A.

β-effect (Munk and Phillips, 1968; Fu, 1981) and to the spectral characteristics of the local wind forcing (Kundu and Thomson, 1985).

Inertial waves observed at a particular place can be either locally generated by the wind or remotely generated at lower latitudes as random internal waves with turning latitudes[3] close to the observation site (Fu, 1981; Munk, 1980). Within the mixed layer, inertial currents are predominantly generated by fluctuations in the local wind stress (Pollard and Millard, 1970). Inhomogeneities in the mixed layer mean circulation can, however, modulate the strength and the effective frequency of the wind-driven inertial oscillations (Weller, 1982; Kunze, 1985).

The decay of mixed layer inertial currents is complex. Surface inertial energy can be destroyed by the wind or propagate downward and equatorward as internal waves (D'Asaro, 1989). Nonlinear interactions with higher frequency internal waves (McComas and Müller, 1981) and with subinertial motions (Weller, 1982) can contribute to the decay. Inertial energy can also be dissipated by instability of the inertial shear at the base of the mixed layer (D'Asaro, 1985). Thus, inertial waves represent a major flux of energy from external sources (i.e., the wind forcing) into the deep ocean which is available for generation of turbulence and mixing.

In the southern California Current System (CCS), observations of inertial or tidal currents go back to the early 1950s. Reid (1962) reports on measurements of surface currents with a geomagnetic electrokinetograph (GEK) at 30N at a distance of 650 km from shore. The observed surface currents showed significant diurnal oscillations which were interpreted as inertial currents driven by the diurnal tide. No evidence against wind generation is, however, given and we personally believe that the local wind forcing is the preferred generation mechanism rather than the diurnal tide. Neutrally-buoyant floats between 500- and 2500-m depth near latitude 30N also showed anticyclonic orbits at speed of 5–18 cm s^{-1} and with a period of about one day (Knauss, 1962). More recently, observations of near-inertial currents were made from the Research Platform FLIP in the same region (Weller, 1985). The strong (maximum speed of 40 cm s^{-1}) near-inertial oscillations were not tide-related and the local wind alone had neither the strength nor the variability needed to directly produce the observed variability. Weller (1985) suggested that the shear of the mean circulation was responsible for the localized intensifications of near-inertial motion.

In this paper, we present a novel way of looking at mixed layer dynamics by analyzing the near-inertial/diurnal motions in the trajectories of surface mixed layer drifters in the CCS between 19N and 36N. The drifter configuration and the drifter data set are briefly described in Section 2. Lagrangian rotary spectra (Section 3) and complex demodulation techniques (Section 4) are used to estimate the frequency and

3. The turning or inertial latitude is the latitude at which the wave frequency is equal to the inertial frequency.

amplitude of the oscillations. The variability of the observed motions is compared to the predictions of a simple model of wind-driven inertial currents (Section 5). In Section 6, three major events of large near-inertial/diurnal currents are studied in detail. The interaction with the background mean surface circulation is discussed. Finally, Section 7 summarizes the essential results gained in our study.

2. Data

The mixed layer drifters deployed in the CCS were of TRISTAR types with a three-axis symmetric drogue at a nominal depth of 14.8 m. A complete description of the drifter systems and a discussion on their water-following capabilities are given in Niiler *et al.* (1987). A downwind slip relative to the water of less than 2 cm s^{-1} is expected.

The drifters were tracked with the ARGOS satellite system. Position fixes averaged 5 per day, with position accuracies of about 250 m. Velocities were computed from consecutive pairs of positions and were assigned a position and time midway between the two fixes. A pessimistic bound of about 5 cm s^{-1} for the velocity errors was estimated by Poulain and Niiler (1989).

A first set of 20 drifters was released during leg I of the FRONTS cruise in July 1985 (Haury *et al.*, 1986). They were deployed in a persistent, seasonally-recurring front in the CCS southwest of San Diego, California (Niiler *et al.*, 1989). Nine other drifters were deployed in March 1986 during the SQ86 cruise near the shore of central California (Hayward *et al.*, 1987). The two drifter data sets are hereafter named after the year of their release.

A description of the 1985 and 1986 drifter trajectories is presented in Poulain *et al.* (1987). Small wiggles or loops appear intermittently in the tracks; these high-frequency motions are the subject of the present study. Drifter trajectories shorter than a month will not be considered. This reduces the total number of drifters to 23. Time is given in days of the year of the drifter deployments (e.g., day 265 for the 1985 drifters is day 265 of year 1985).

Surface winds over the CCS, representative of nominal 19.5-m anemometer heights, were obtained from the Fleet Numerical Oceanography Center (FNOC). Using a planetary boundary layer model and various field observations (FNWC, 1975), the FNOC provides wind analyses every 6 hours on a northern hemisphere polar stereographic grid. Grid spacing over the CCS is about 300 km. Comparisons with direct buoy observations of winds (Pazan *et al.*, 1982) indicate that the FNOC winds are generally lower in variance than the actual observations. Wind speed at 10-m height was computed using the logarithmic wind profile (Tennekes and Lumley, 1987). Wind stress at the ocean surface was calculated using the wind speed-dependent drag coefficient suggested by Large and Pond (1981).

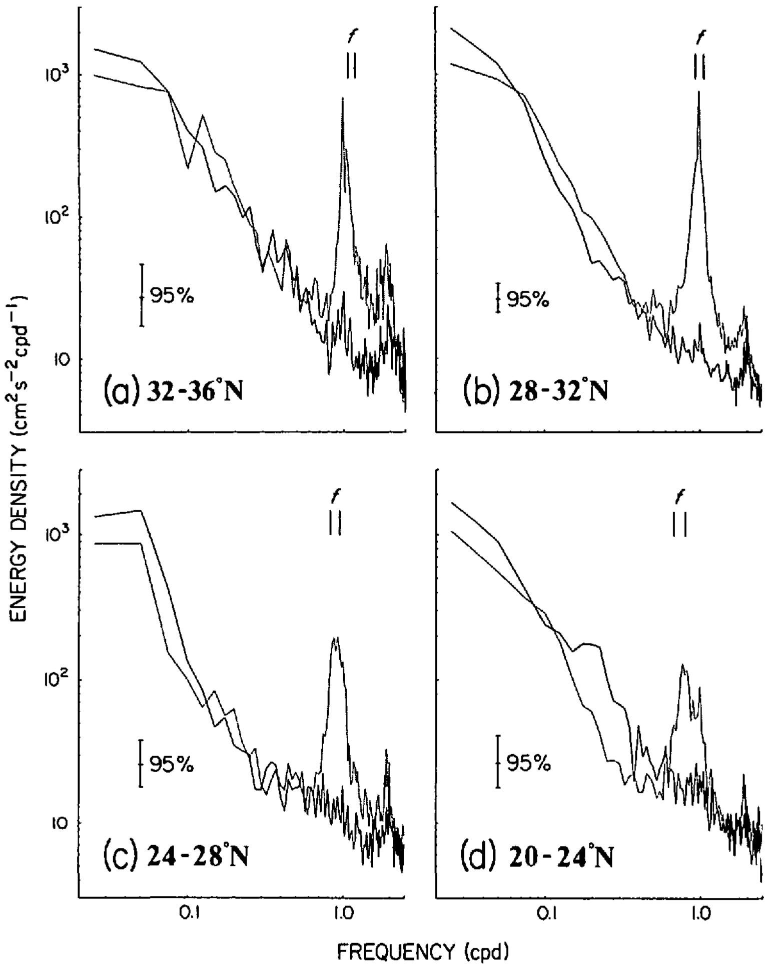

Figure 1. Lagrangian rotary spectra (solid: anticlockwise, dotted: clockwise) from the drifter observations in the 32–36N (a), 28–32N (b), 24–28N (c) and 20–24N (d) latitude bands.

3. Lagrangian rotary spectra

The mean distribution of kinetic energy of the horizontal currents as a function of time scale was computed using rotary spectra (Gonella, 1972). The raw drifter velocity time series were first linearly interpolated every 0.2 day. This procedure reduced the velocity variance by about 20%. Each velocity time series was chopped into subseries of 40 days which were sorted into latitude bands of 4° according to the location of the first velocity estimate in each of them. Figure 1 presents the Lagrangian rotary spectra in four latitude bands. The spectra are essentially red with a strong peak corresponding to clockwise oscillations at near-inertial or diurnal frequencies. Small semi-diurnal peaks also appear in both the clockwise and anticlockwise components of the spectra. For periods greater than 10 days, the anticlockwise component is larger than the clockwise component. This indicates a preferential anticlockwise sense of rotation of the large-scale/low-frequency fluctuations (Poulain and Niiler, 1989). The inertial peak follows the local inertial frequency. Moving south, the peak weakens and becomes comparable in magnitude to the adjacent diurnal peak which can be barely resolved in the lowest latitude band (20–24N).

4. Complex demodulation

In order to determine the spatio-temporal variations of the near-inertial and diurnal components of the observed currents, we applied a band-pass filter to the drifter velocity time series. The method used is a generalization of complex demodulation (Tukey, 1961) to allow for slow time variation of the demodulation frequency. Details can be found in Appendix 1.

Given the broad band and the relatively small signal-to-noise ratio (see below) of the near-inertial/diurnal signal, we decided to adopt a boxcar window [$w(t) = 1$ over a moving interval of length $2T = 10$ days centered at each observation] in the complex demodulation. The choice of $T = 5$ days is necessary to reduce leakage from other frequency bands into the demodulated signal. The drawback with using such a long data window is that there is more smoothing in time and that temporal resolution is decreased as a result. We will see, however, that events of large near-inertial/diurnal oscillations typically last 10 days so they are well resolved with a boxcar window of 10 days.

The amplitude of the demodulated currents at the local inertial frequency is plotted versus time in Figures 2 and 3 for the 1985 and 1986 drifters, respectively. The temporal distribution of inertial currents in the mixed layer of the CCS appears very intermittent. In addition to numerous oscillations at periods of 5–10 days which arise probably from leakage problems, events of relatively strong inertial currents with amplitudes ranging from 10 to 20 cm s^{-1} exist between days 200 and 300 in the majority of the 1985 tracks. For the 1986 drifters, large inertial oscillations are dominant between days 150 and 200. All these events are characterized by a signal-to-noise ratio of about 5.

Since our data set is Lagrangian, the variabilities of the inertial currents are intrinsically temporal and spatial. In order to show the spatial variations of the demodulated currents, we have plotted the trajectories of the 1985 (Fig. 4) and 1986 (Fig. 5) drifters using a line thickness proportional to the amplitude of the inertial currents. Inertial oscillations with substantial amplitude appear mostly near the coast. Globally, the amplitudes decrease moving west and south. No significant inertial oscillations are found south of 24N ($y = -700$ km).

5. Wind-driven inertial oscillations

It is well known that the local wind forcing is the major generating mechanism of inertial oscillations in the surface mixed layer (e.g., Pollard and Millard, 1970; Pollard,

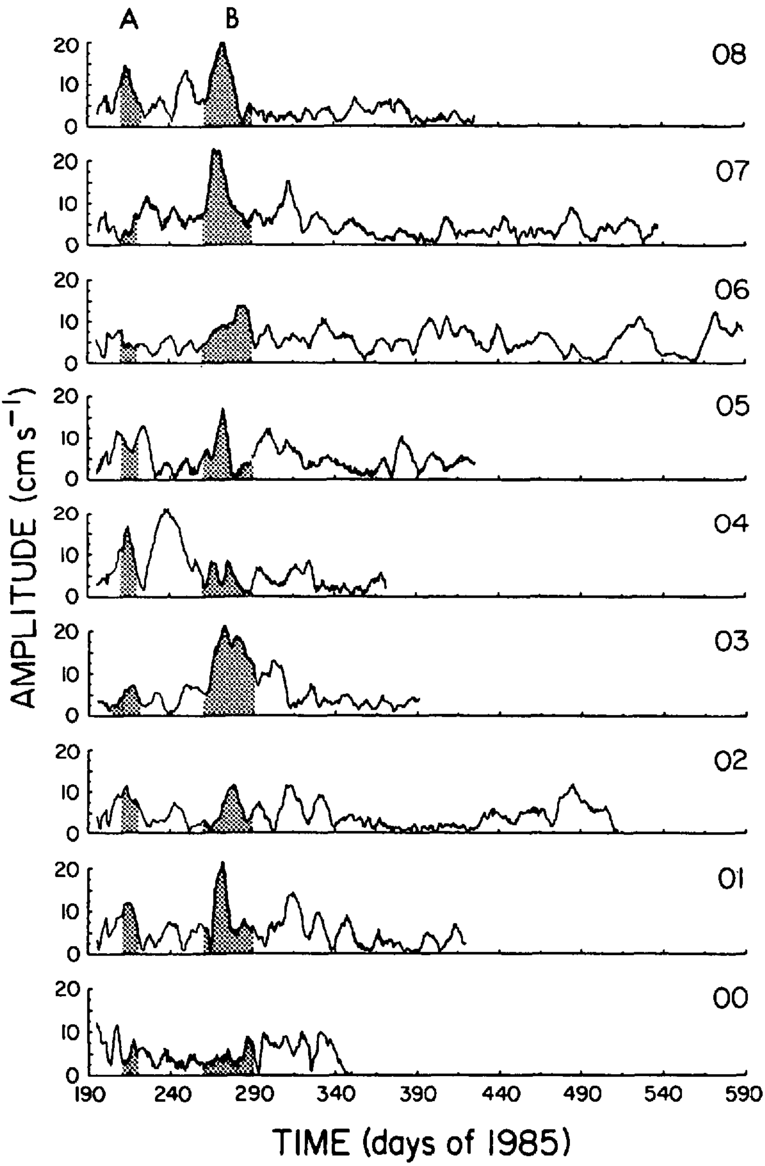

Figure 2. Time series of the inertial current amplitudes for the 1985 drifters. The two events (A and B) discussed in the text are marked with stippled areas.

1980). We, therefore, propose to relate the observed inertial motions to fluctuations in the local wind stress. A simple damped slab model of the mixed layer (Pollard and Millard, 1970) is used

$$\frac{d}{dt}\mathbf{u}(t) + 2\pi(if(t) + r)\,\mathbf{u}(t) = \frac{\tau(t)}{\rho h}, \tag{1}$$

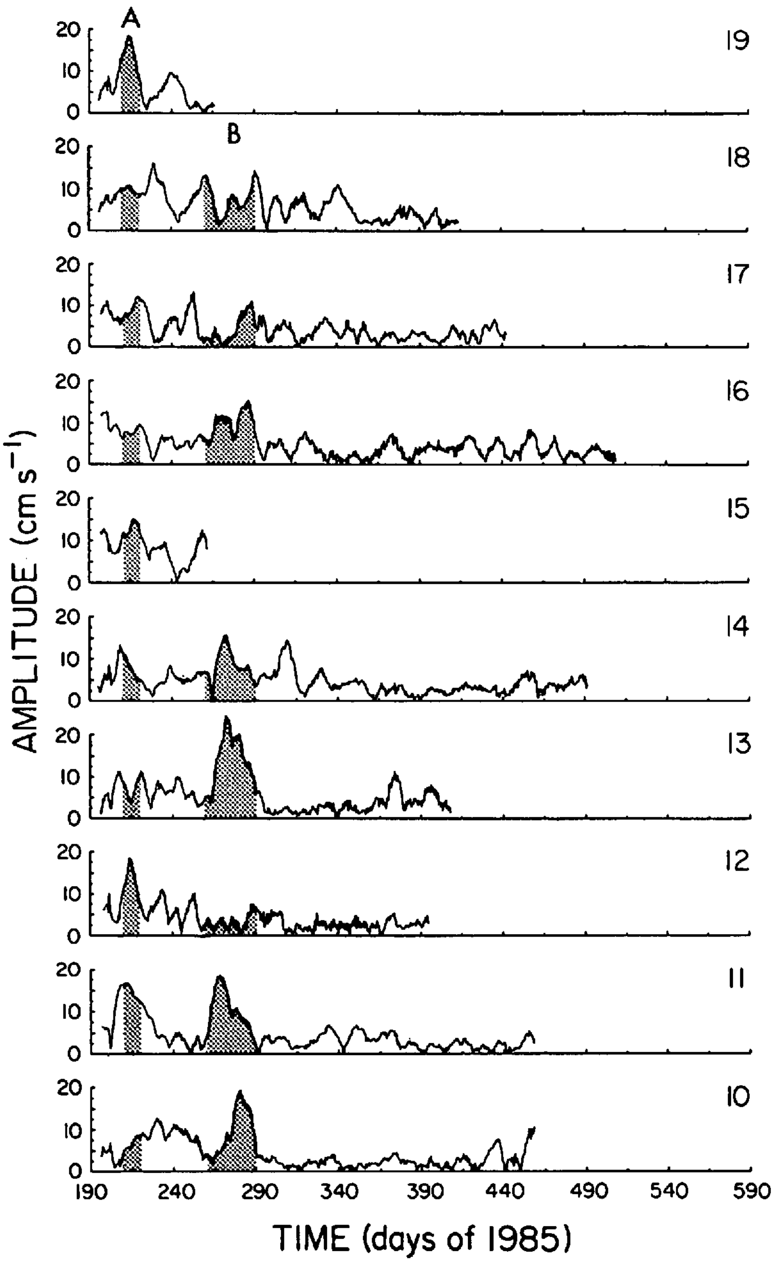

Figure 2. (Continued)

where $\mathbf{u}(t) = u(t) + iv(t)$ is the horizontal velocity within the mixed layer, $\tau(t) = \tau_x(t) + i\tau_y(t)$ is the wind stress at the surface, $f(t)$ is the local inertial frequency, r is an arbitrary decay constant and h is the depth of the mixed layer of density ρ.

The wind stress calculated from the FNOC 6-hourly wind products is not a reliable

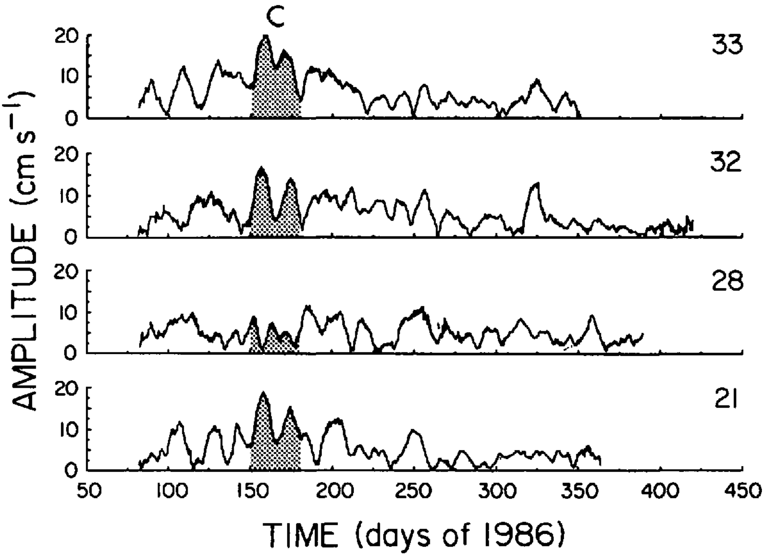

Figure 3. As Figure 2 but for the 1986 drifters. Event C is marked with stippled areas.

indicator of the actual wind stress fluctuations at periods less than a day (Thomson, 1983). This data set is, therefore, not appropriate for studying the wind-driven inertial currents for which fluctuations in the wind field at periods less or equal to one day may be very important. Besides, data is generally not available on the velocity vertical structure in the vicinity of the drifters and the mixed layer depth h remains unknown. The FNOC wind stress and the simple slab model (1) are, therefore, used only to explain qualitatively the spatio-temporal distribution of the inertial current amplitudes.

The surface wind stress was linearly interpolated in space and time to the drifter coordinates. Model (1) was then applied with $h = 20$ m and $r^{-1} = 20$ days. The first value is typical in the southern CCS for the summer and fall seasons (Lynn *et al.*, 1982). The latter was chosen to match the longest time scale of the large inertial current events observed in the drifter tracks. The modeled currents were demodulated at the local inertial frequency in exactly the same way as for the observed currents. Time series of the observed and modeled inertial current amplitudes, and of the interpolated wind stress, are depicted for some of the drifters in Figures 6 and 7.

Correlation coefficients between observed and modeled amplitudes over the whole time series are presented in Table 1. They vary from 0.63 (drifter 13) to 0.91 (drifter 32). This is quite remarkable in view of the poor quality of the wind data and the simplicity of model (1). The substantial discrepancies between the predictions and the actual inertial current amplitudes, such as for drifter 3 around day 290 and drifter 28 around day 160, may be due to (1) the effect of unresolved small-scale structures in the wind field, (2) the interaction with patterns in the mixed layer mean circulation, and

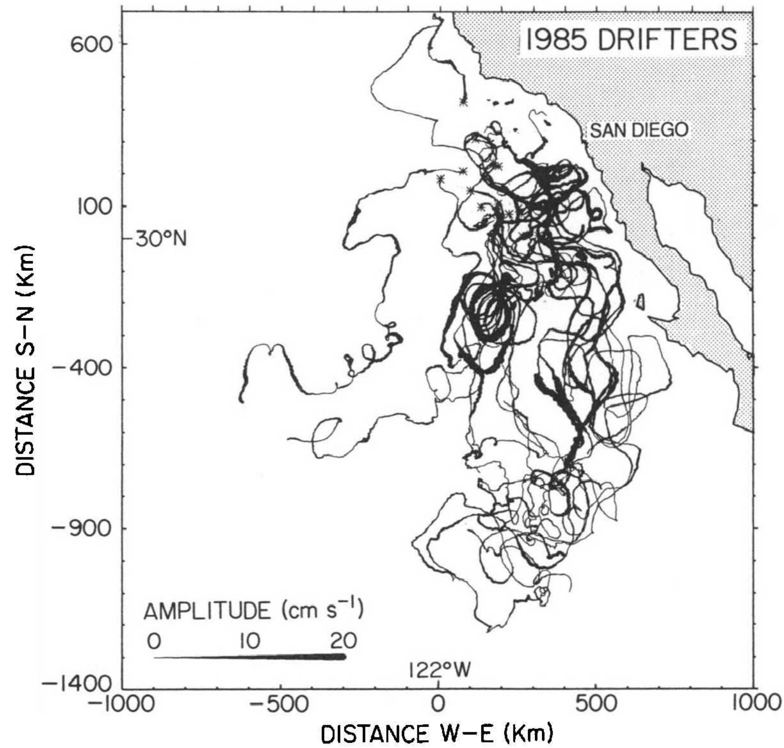

Figure 4. Spatial distribution of the inertial current amplitudes (shown as the thickness of the tracks) for the 1985 drifters. Deployment locations are depicted with star symbols.

(3) the nonlocal generation of inertial waves. Some of these issues will be discussed for specific events of large inertial oscillations in the next section. Despite many discrepancies between the observed and modeled inertial currents, our results (Figs. 5 and 6, coefficients in Table 1) confirm that the local wind stress plays a major role in the generation of inertial oscillations observed in the drifter tracks.

6. Major near-inertial/diurnal current events

In this section, we study in detail three major events of large (maximum amplitude greater than 15 cm s^{-1}) near-inertial/diurnal currents (denoted A, B and C in Figs. 2 and 3). Since the observations were taken in a latitude range which includes the turning latitude 30N, near-inertial and diurnal frequency bands can be close or equal to each other. Both bands can have substantial energy levels (see Fig. 1). The best way to separate the energy levels in the peaks is to use the technique of simultaneous demodulation at two frequencies (see Appendix 2). As for the demodulation at one frequency, the characteristic time scale and the small signal-to-noise ratio of the near-inertial/diurnal signal require a demodulation with a boxcar time window of length $2T = 10$ days. For the case of oscillating currents at the diurnal frequency,

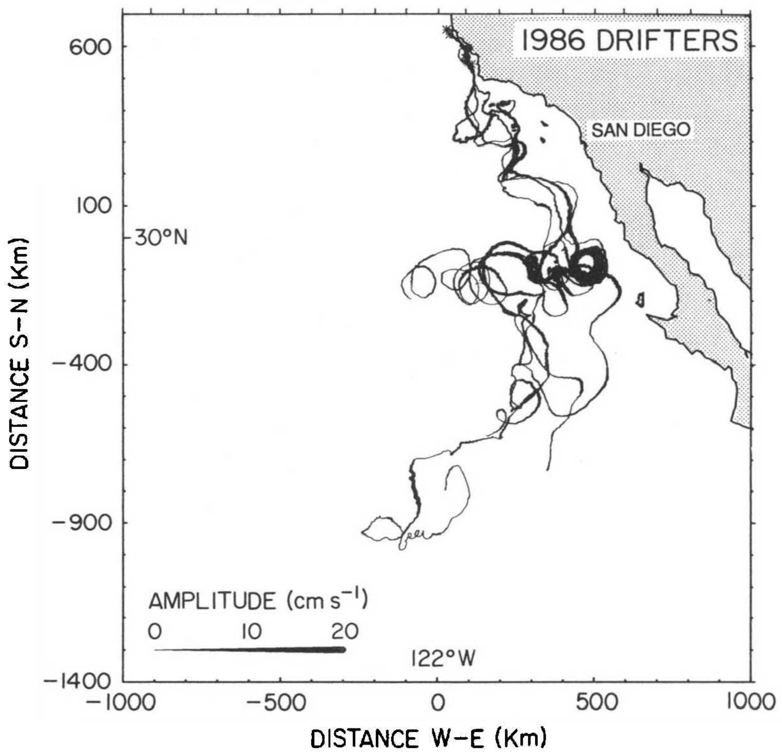

Figure 5. As Figure 4 but for the 1986 drifters.

there is a priori no preferential sense of rotation and the currents are not generally circularly polarized. It will be, therefore, interesting to examine the characteristics of the diurnal current ellipse (see Appendix 3).

a. Event A (diurnal). The first substantial event of large oscillations appears around day 215 (3 August 1985) for more than half of the 1985 drifters (see Fig. 2). The simultaneous demodulation at the local inertial and diurnal frequencies reveals that the event consists essentially of oscillations at the diurnal frequency. The lengths of the semi-principal axes of the tidal ellipse are shown in Figure 8. The minor axis is consistently positive corresponding to clockwise rotation of the current vector. For drifters 4, 18 and 19, the motions are essentially circularly polarized. In contrast, significant ellipticity is found for drifter 9, 12 and 15 and the orientation of the ellipse varies from the zonal (drifters 12 and 15) to the meridional directions (drifter 9). The spatial variations in ellipticity are possibly related to the structure of diurnal wave beams on the continental shelf (Prinsenberg *et al.*, 1974) but, given the paucity of the observations, this is pure speculation. The time scale of the event is about 10 days.

The spatial distribution of the diurnal oscillations is depicted in Figure 9. Maximum amplitudes are found on the continental shelf off Baja California a few degrees north of

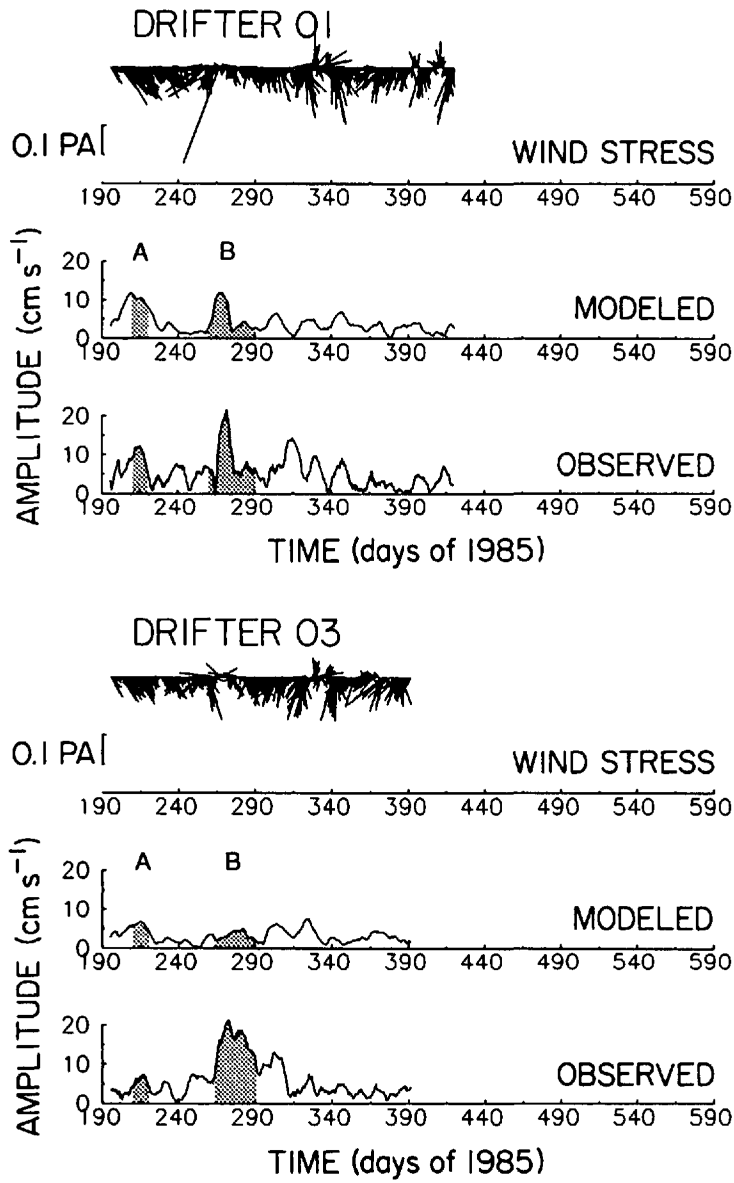

Figure 6. Observed and modeled amplitude of inertial currents in the mixed layer for 6 of the 1985 drifters. The wind stress vector is represented with sticks every 6 hours.

30N (15–20 cm s^{-1} for drifters 4, 9, 12, 15, 18 and 19). The phase of the diurnal oscillations decreases northward along the coast. The corresponding speed of northward propagation is of the order of 10 m s^{-1}. This is at least an order of magnitude smaller than the speed of propagation of the diurnal tide currents on the continental

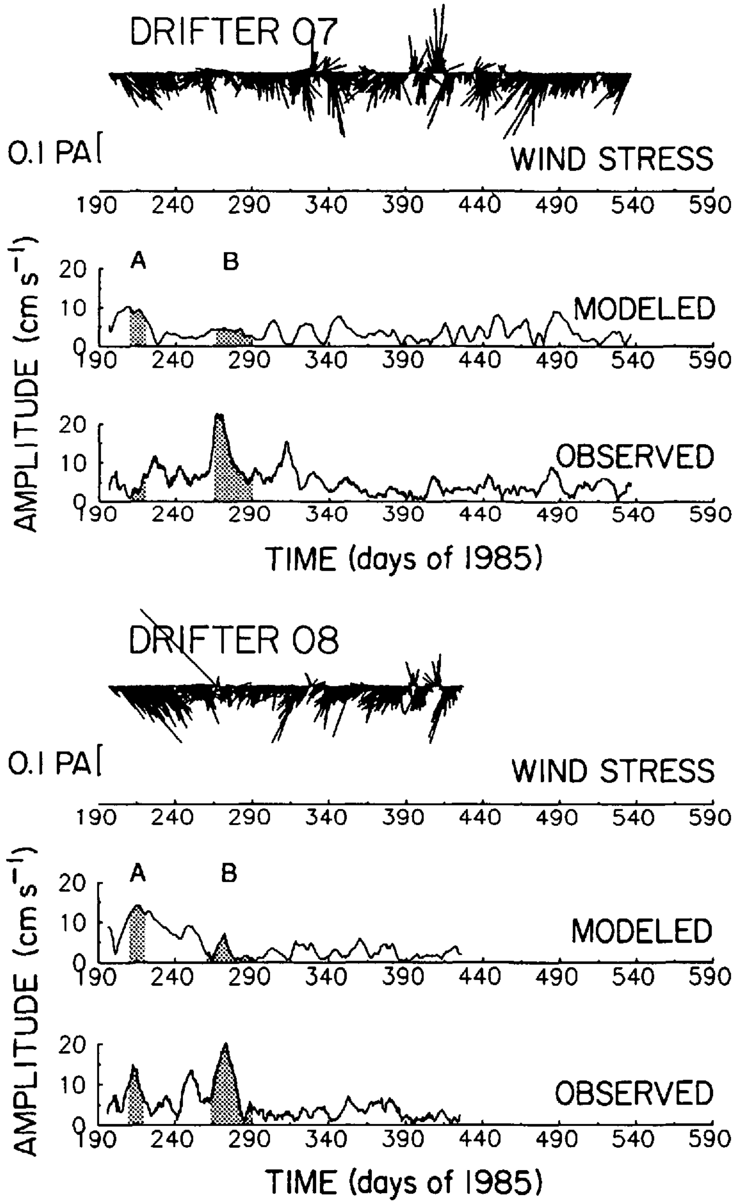

Figure 6. (Continued)

shelf (about 200 cm s^{-1}, see Munk *et al.*, 1970). Thus, the observed diurnal currents do not seem to be phase-locked to the diurnal tide.

The slab model (1) predicts strong wind-driven diurnal oscillations for the time period corresponding to the event (Fig. 6). The spatial structure of the wind stress field (not illustrated) shows that this event follows an intensification and clockwise rotation

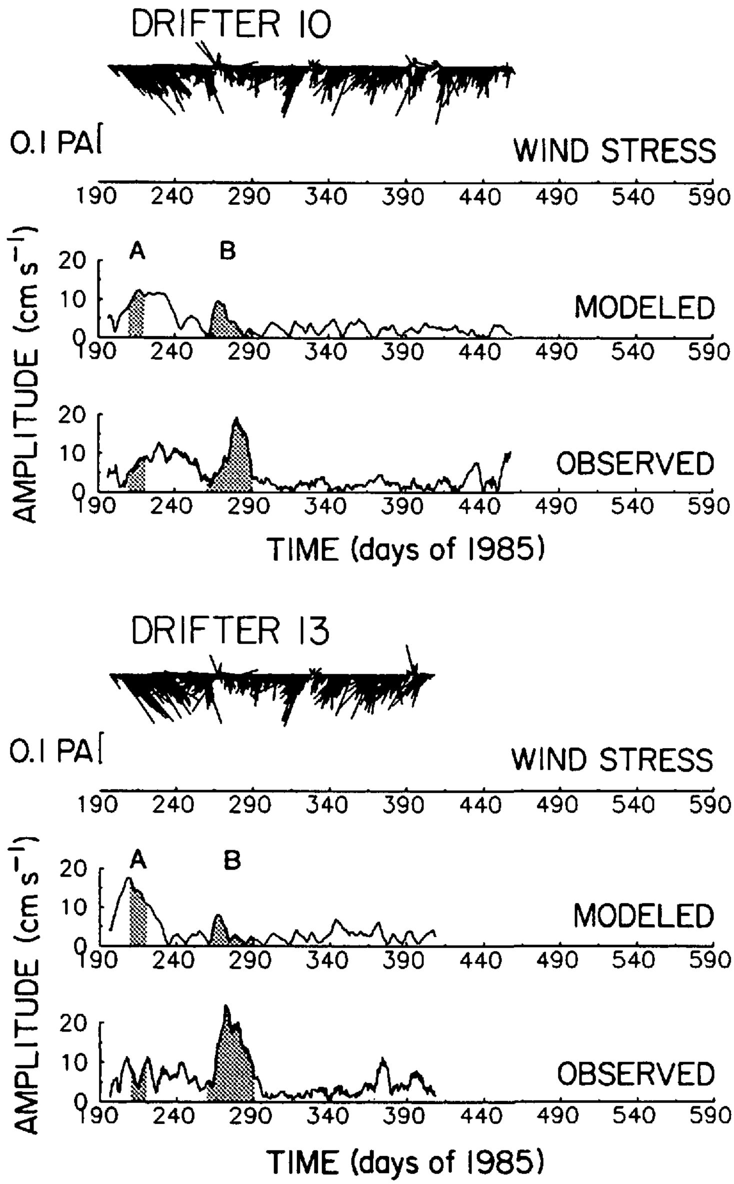

Figure 6. (Continued)

of the northwesterly winds within 500 km of the shore. This indicates that the diurnal currents are related to the local wind forcing.

b. Event B (near-inertial). A major event appears in more than half of the 1985 drifter tracks between days 260 and 290 (late September and early October 1985). Drifters 0,

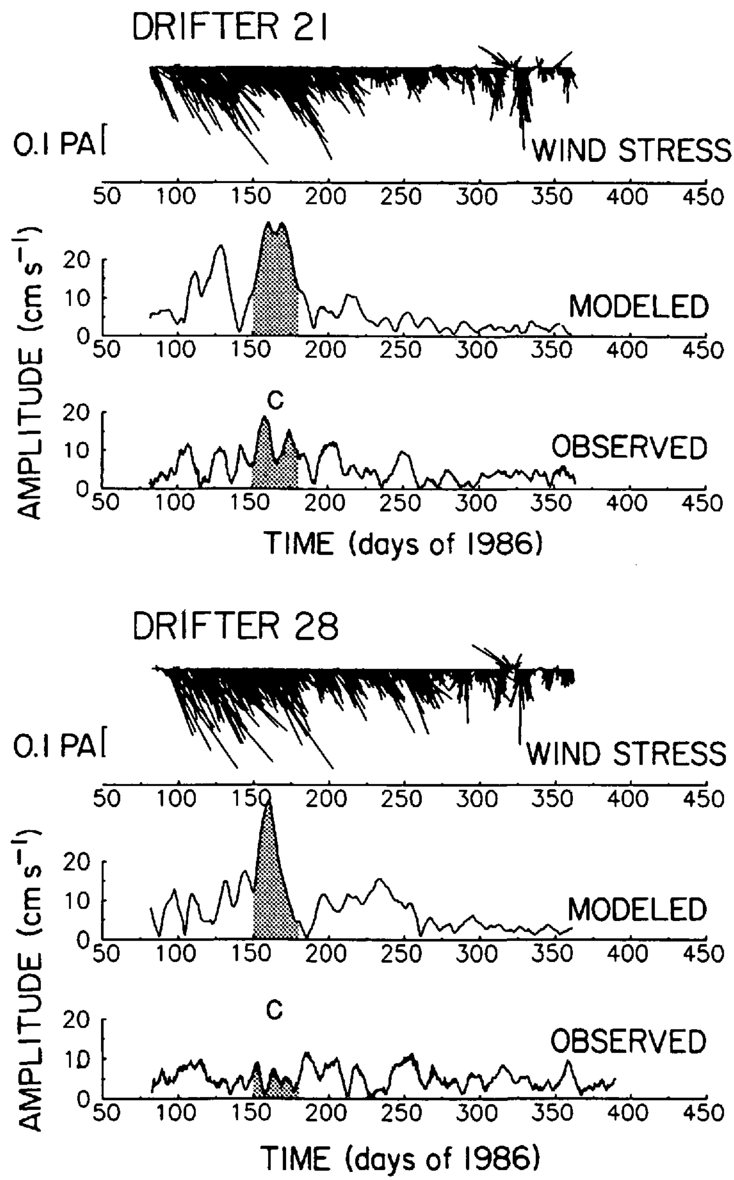

Figure 7. As Figure 6 for the 1986 drifters.

4 and 12 are the only ones with no signature of the event. Using the technique of simultaneous demodulation at two frequencies, we found that the event is essentially inertial. The geographical distribution of the amplitude of the inertial currents (estimated by the demodulation at one frequency) and of the FNOC wind stress is presented in Figure 10. A low-pressure system with strong cyclonic winds is evident in the vicinity of the drifters. This tropical storm sweeps by the drifters in a couple of days

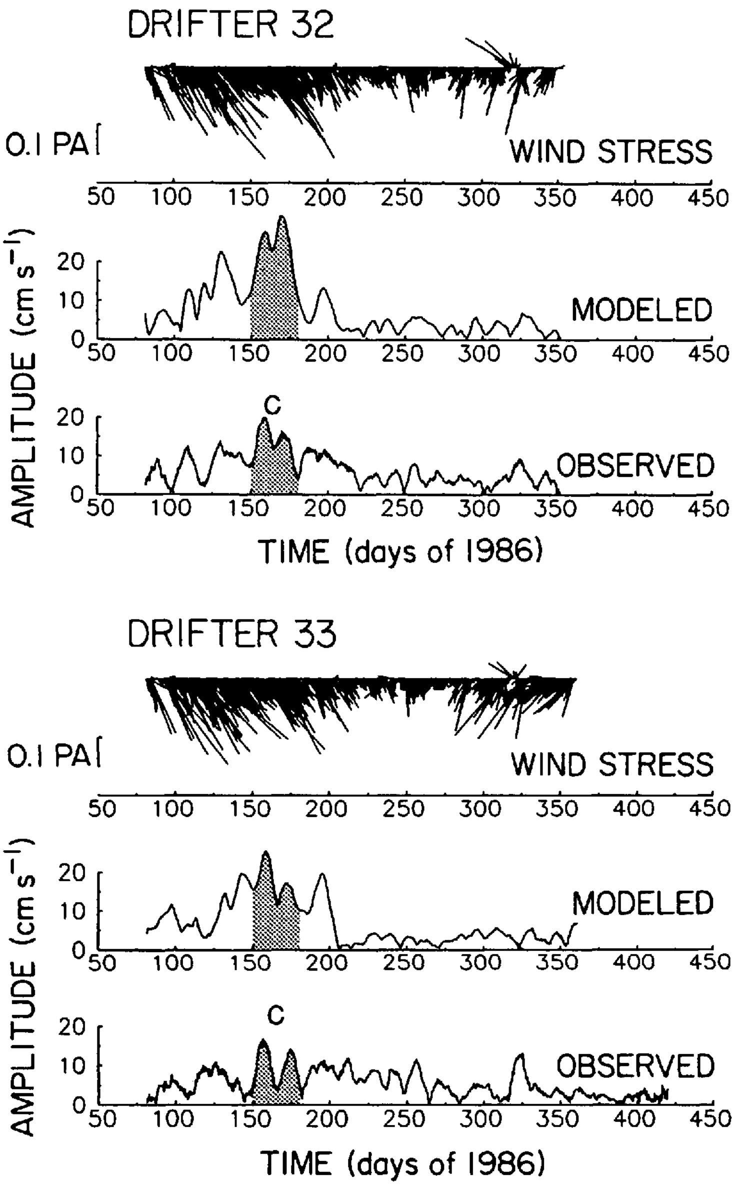

Figure 7. (Continued)

(days 266–268) moving to the northwest. On day 269, the system has decayed and the winds are uniformly calm. This feature in the surface winds is roughly simultaneous with the large inertial oscillations in the drifter trajectories. More precisely, near-inertial oscillations tend to be first triggered in the drifters to the southwest [drifters 1, 7, 11] around day 263 and then appear later (day 265) in drifters more to the northeast

Table 1. Correlation coefficients between the observed and modeled inertial current amplitudes over the whole time series.

Drifter number	Number of observations	Correlation coefficient
01	1061	0.82
03	966	0.75
07	1838	0.70
08	1171	0.78
10	1295	0.73
13	1025	0.63
21	1749	0.85
28	1977	0.67
32	1747	0.91
33	2104	0.78

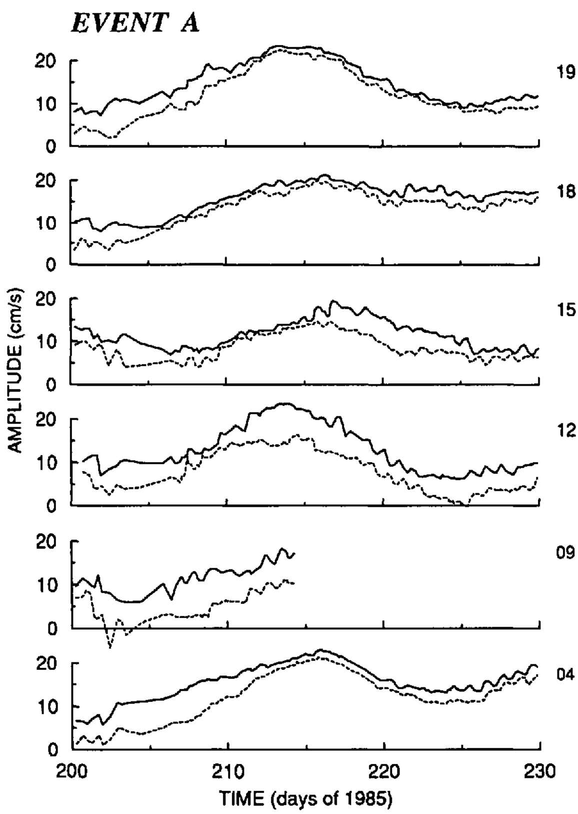

Figure 8. Time series of the semi-principal axes (major: solid, minor: dashed) of the diurnal current ellipse for 6 of the 1985 drifters during event A.

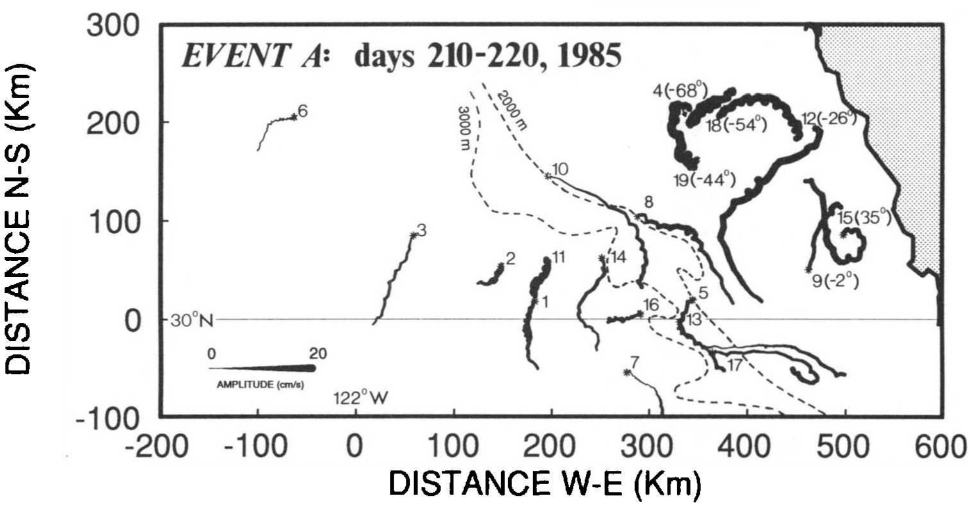

Figure 9. Spatial distribution of the diurnal current amplitudes for event A: days 210–220, 1985. Star symbols and drifter numbers are posted at the beginning of each 10-day-long track. The phases of the motions are shown between parentheses. The continental slope is depicted by the 2000 and 3000 m isobaths (dashed lines).

[e.g., drifters 3, 5, 14] (see Fig. 11). For this period (days 263–365) the center of the storm is located more than 500 km to the south of the drifter region, but amplification and clockwise rotation of the wind stress vector is evident above the drifters. Thus, there is a qualitative agreement between the northwest motion of the wind patterns and the triggering of near-inertial currents in the drifter trajectories.

It is remarkable that inertial currents can be very different for drifters in the same vicinity. The best example of high horizontal gradient of inertial energy is for drifters 10 and 13 between days 265 and 275. The variation in amplitude is 15 cm s^{-1} over only 50 km. This contrast in drifter behavior disappears around day 280 with the onset of a large signal of inertial oscillations in both trajectories (see Figs. 2 and 11). The absence of energy in the inertial frequency band for drifter 10 around day 270 is not explained by our simple model of locally wind-driven inertial currents (see Fig. 6).

We now propose a possible interpretation of the different energy levels in drifters 10 and 13 based on the interaction with the mean flow patterns. Information on the mesoscale circulation in the region sampled by the drifters was obtained from a satellite infrared image of the sea surface before the storm cloud system overcasts the drifters (Poulain, 1989). The image shows that drifter 10 makes half a cyclonic loop in a 50-km scale warm eddy. In contrast, there is no striking feature in the mesoscale circulation around drifter 13 (slow southward flow). The absence of oscillations when drifter 10 is caught in the eddy is compatible with the positive vorticity of the mesoscale feature. Indeed, inertial waves generated in regions of positive vorticity are less inertial outside the region and will propagate rapidly out of the positive vorticity. Furthermore,

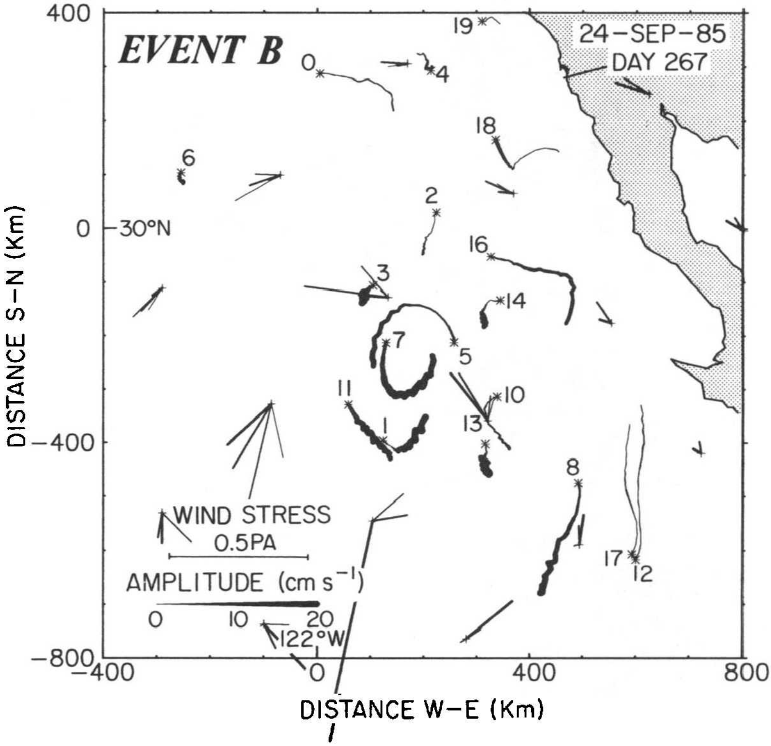

Figure 10. Spatial distribution of near-inertial oscillations in the drifter trajectories for 10 days around day 267 of 1985 (event B). The track thickness is proportional to the inertial current amplitude. Star symbols and drifter numbers are posted at the beginning of each track. The wind stresses at 0000 (thick), 0600, 1200 and 1800 (thin) UT of day 267 are represented with sticks at the FNOC grid points.

inertial waves cannot propagate into the positive vorticity region because their frequency is lower than the effective inertial frequency in the eddy (Kunze, 1985).

The determination of the actual frequency of the oscillations is not an easy task given the possible existence of energy in the diurnal band and the poor resolution in frequency imposed by the intermittent character of the event. In order to estimate the frequency of oscillation, we modified the demodulation procedure to maximize the variance explained by the oscillation. For each 10-day interval, the signal was demodulated at the frequencies between 0.5 and 1.5 cpd (with an increment of 0.01 cpd). The frequency and amplitude corresponding to the maximum explained variance (or maximum skill, see Appendix 1) only were retained. They are depicted with solid lines in Figure 11 for nine of the 1985 drifters. The simultaneous demodulation at the diurnal frequency and at an unknown frequency (tuned to maximize the explained variance) was also performed. This procedure works fine away from the inertial latitude, e.g., outside the latitude band 28°30′N-31°30′N where the determinant of matrix M is greater than 0.5 (see Appendix 2). The results are shown with symbols in Figure 11.

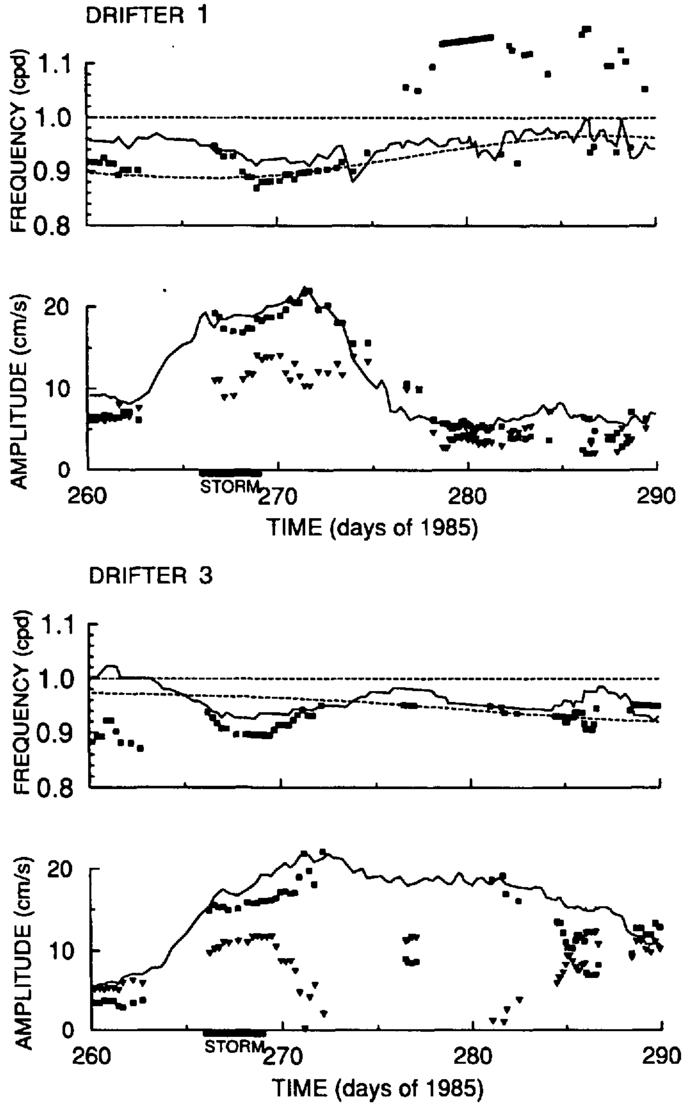

Figure 11. Amplitude and frequency of the near-inertial and diurnal oscillations between days 260 and 290 of 1985 (event B) for the drifters with significant signature of the event. Solid line: demodulation at one frequency. Symbols: Simultaneous demodulation at the near-inertial (squares) and the diurnal (triangles) frequencies, results are only shown when det(M) > 0.5 (see Appendix 2). The diurnal and local inertial frequencies are also depicted with dashed lines.

The difference between the inertial and actual frequencies, estimated with the demodulation at one frequency, can be the effect of substantial energy in the higher frequency diurnal band (see drifters 1, 7 and 11). Also, two distinct peaks of medium amplitude (10 cm s^{-1}) can give a large event (20 cm s^{-1}) in the demodulated signal at

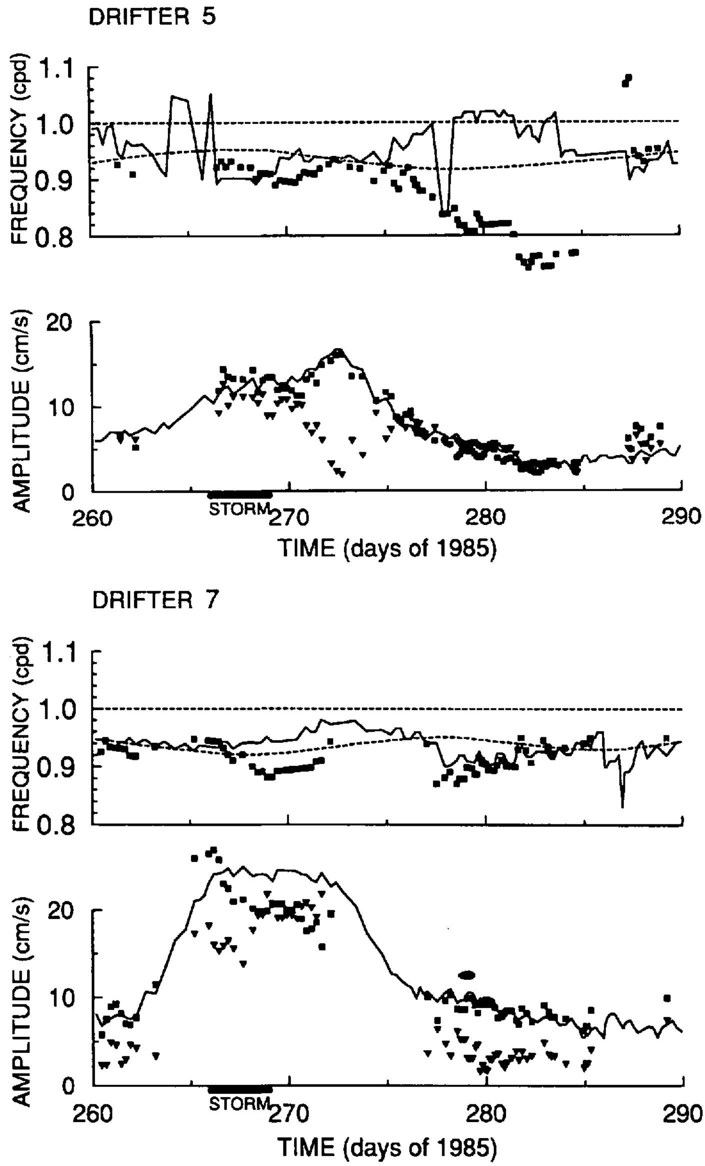

Figure 11. (Continued)

one frequency if the diurnal and inertial frequencies are close to each other (see drifter 3 around day 278). Therefore, an accurate determination of the amplitude and frequency of the near-inertial currents in the presence of diurnal energy can only be done by demodulating simultaneously at the diurnal and near-inertial frequencies. We estimated the accuracy of the frequencies presented in Figure 11 to be 0.01–0.02 cpd.

Figure 11 shows that, in general, the event is centered on day 270 (just after the

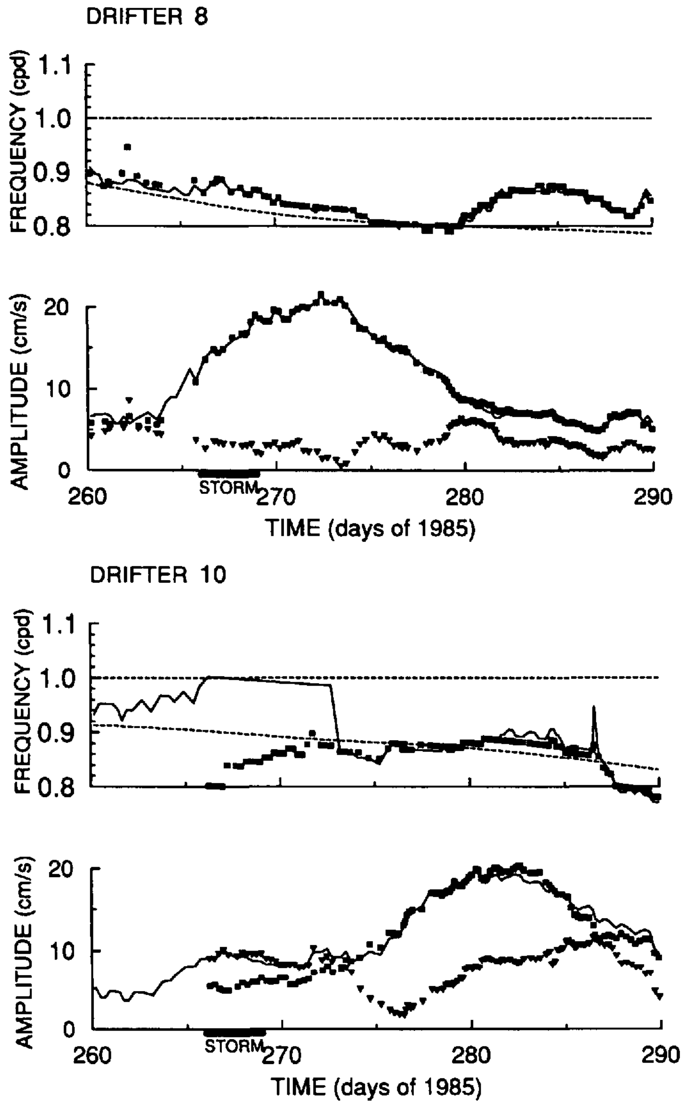

Figure 11. (Continued)

storm) and that it has a time scale of about 10 days. Exceptions are found for drifter 10 with a 10-day long event centered on day 280, and for drifter 13 which has an event lasting almost for 20 days. We suspect that the event in drifter 13 can be divided into two subevents, the second one being centered around 280 and being similar to the one in drifter 10.

The distribution of energy between the near-inertial and the diurnal bands varies from an almost equal partition of energy (drifters 5, 7 and 14) to no significant energy

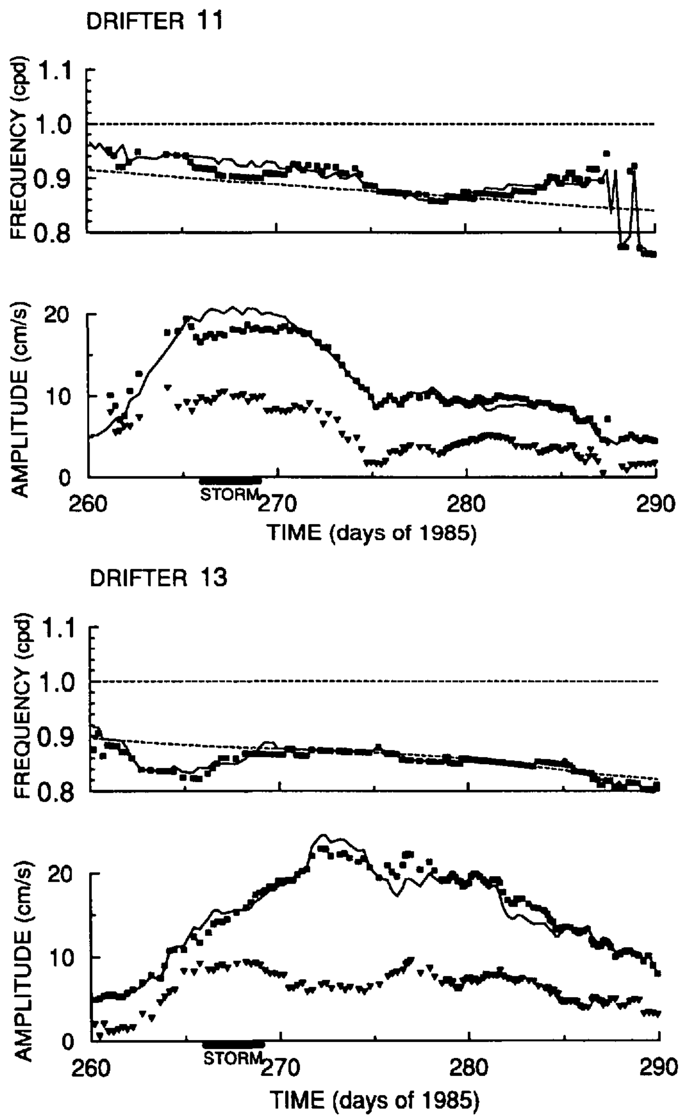

Figure 11. (Continued)

in the diurnal band (drifters 8 and 13). The actual frequency of the oscillations varies as a function of time. It can differ from the local inertial frequency by as much as 0.07 cpd (drifter 3 around day 268).

Substantial red shifts are found for drifters 3, 5, 7 and 14. Red shifting of the inertial frequency is mainly due to interactions with the background mesoscale circulation. More specifically, the vorticity of the mean flow ζ is known to shift the frequency of inertial response to $f + (2\pi)^{-1} \zeta/2$ (Weller, 1982; Kunze, 1985). Thus, the typical

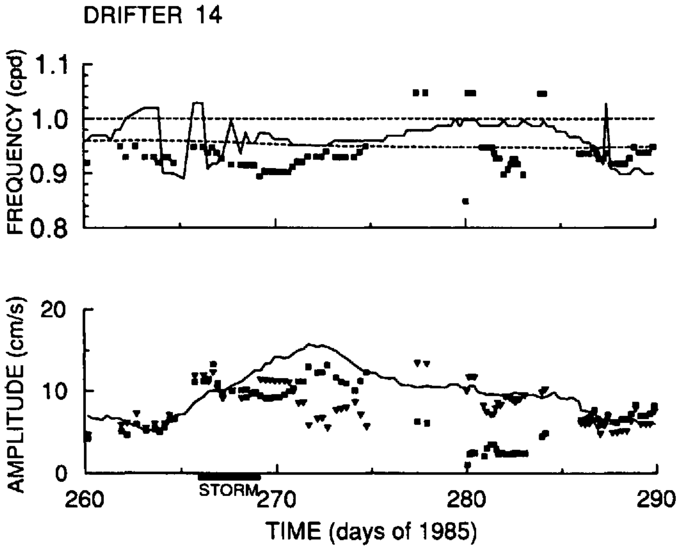

Figure 11. (Continued)

observed frequency shift (-0.05 cpd) can correspond to a vorticity of about $-0.7 \times 10^{-5}\, s^{-1}$. Figure 10 shows that the above drifters are in the region of a strong cyclonic eddy. The negative vorticity estimated from the red shifts indicates that the drifters are in the outer edge of the cyclonic eddy (region of negative vorticity). The value of this vorticity can be roughly estimated as follows: Consider drifters 3 and 7 around day 270. Their orbital speeds are 6 and 23 cm s^{-1}, respectively. Dividing the difference of these speeds by the distance between the two drifters (70 km) yields $-0.2 \times 10^{-5}\, s^{-1}$ for the vorticity. The two estimates of vorticity are of the same order of magnitude. The observed red shift of the inertial frequency is, therefore, qualitatively consistent with the local vorticity of the mean flow.

Actual frequency significantly above the local inertial frequency is found at the beginning of the event in drifters 1 and 7, and for drifters 8, 10 and 11. Maximum blue shift is about 0.05 cpd. The interpretation of the blue shift of the inertial frequency is not attempted here since it can be the result of many unknown factors, i.e., the interactions with the mean circulation, the characteristics of the wind forcing and the β-effect (Fu, 1981).

c. Event C (diurnal). The most striking event of large near-inertial/diurnal currents in the 1986 drifter trajectories occurs between days 150 and 180 (June 1986, see Fig. 3). After demodulation at the diurnal and inertial frequencies, we found that the event consists of diurnal oscillations. The geographical distribution of the oscillations during the event is shown in Figure 12. Strong motions at the diurnal frequency appear in a 100-km anticyclonic eddy located on the continental shelf about 100 km south of 30N

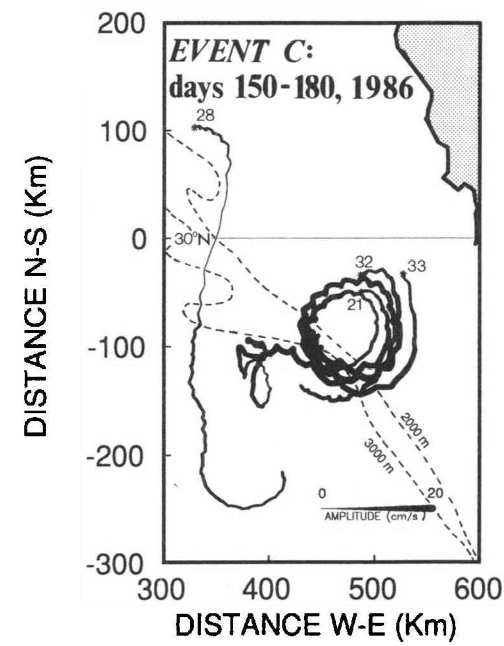

Figure 12. Geographical distribution of the diurnal amplitude for event C: trajectories between days 150 and 180 of 1986. The line thickness is proportional to the amplitude. Star symbols indicate the beginning of each track. The continental slope is depicted by the 2000- and 3000-m isobaths (dashed lines).

(drifters 21, 32, 33). The currents sampled by drifters 21, 32 and 33 oscillate in phase. In contrast, no substantial high-frequency motion is evident in the trajectory of drifter 28.

Strong winds (with a maximum speed of 15 m s^{-1}) are blowing from the northwest in the vicinity of the drifters during the event. Except for drifter 28, our simple model of wind-driven inertial oscillation predicts fairly well the temporal variations in the observed near-inertial current amplitudes (Fig. 7). The absence of inertial or diurnal oscillations in the trajectory of drifter 28 is surprising given the strong response predicted by the model. The available data do not give an explanation of this discrepancy. We suspect, however, that the location of drifter 28 west of the continental slope (Fig. 12) might be important to explain its different behavior compared to the other drifters.

The lengths of the semi-axes of the current ellipse are plotted versus time in Figure 13 for the four 1986 drifters. The event is characterized by two maxima separated by about 15 days. This bimodal structure is also seen in the modeled wind-driven oscillations (Fig. 7) so it is not an effect of energy leakage from other frequency bands but actually two events. Both events have a time scale of about 10 days.

We now focus on the first event centered about day 160 and for which all three

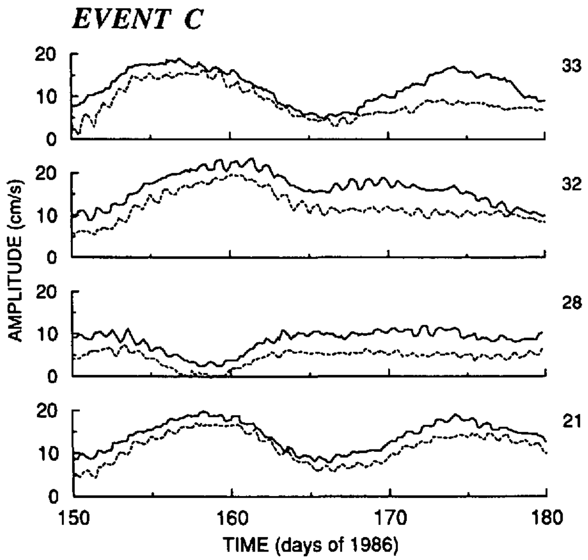

Figure 13. Time series of the semi-principal axes (major: solid, minor: dashed) of the diurnal current ellipse for the 1986 drifters during event C.

drifters (21, 32 and 33) are close to each other in the eddy. The phase, orientation and ellipticity of the current ellipses are similar for the three drifters. The current ellipses are slightly elongated in the meridional direction; the ratio of the minor to major axes varies between 0.8 and 0.9.

The background vorticity, divergence and deformation rates were estimated from the simultaneous relative drifter positions and velocities interpolated at 0.2 day intervals (Molinari and Kirwan, 1975; Niiler *et al.*, 1989). This method gives reliable results for the first part of the event (days 150–155). The mean vorticity is significantly negative with a magnitude of about $10^{-5}\ s^{-1}$. The mean divergence is not significantly different from zero and the two mean deformation rates are about $-5 \times 10^{-5}\ s^{-1}$. The vorticity of the mesoscale flow shifts the lower bound of the internal waveband to an effective frequency $f + (2\pi)^{-1}\,\zeta/2$ approximately equal to $0.98 - 0.07 = 0.91$ cpd. The departure of the actual frequency of the oscillations (1 cpd) from the effective inertial frequency (0.91 cpd) agrees well with the observed ellipticity of the currents. Indeed, according to the theory of linear internal waves, the ratio of the principal axes of the velocity ellipse is equal to the ratio of the (effective) inertial frequency to the frequency of oscillation. In our case, we have 0.91/1.00 and this value is similar to the observed ellipticity.

7. Summary and discussion

Near-inertial and diurnal motions appeared intermittently in the trajectories of mixed layer drifters in the southern California Current System (CCS). The temporal and spatial variations of the energy in the near-inertial/diurnal frequency bands have been analyzed using a generalized complex demodulation technique. A simple slab model of wind-driven currents was used to explain the variability of the observed oscillations. Although there are some discrepancies between the model and the observations, there is a global qualitative agreement between both time series. The local wind stress plays, therefore, a major role in the generation of the drifter near-inertial/diurnal motions.

Although the Lagrangian observations were taken around the inertial latitude 30N, where inertial oscillations are theoretically in resonance with the diurnal tide, no peak of inertial oscillations at 30N is evident. The forcing by the diurnal tide and the resonance mechanism (Hendershott, 1973; Craig, 1989) must be weak compared to the wind forcing.

Two major events of large ($\approx$20 cm s^{-1}) oscillations at the diurnal frequency were observed near 30N on the continental shelf off Baja California. For the first event (*Event A*, August 1985), the frequency of oscillation (1 cpd) is below the local inertial frequency and the motions are circularly polarized and not phase-locked to the diurnal tide. These subinertial waves can be interpreted as shelf waves trapped on the continental shelf (Cartwright, 1969; Munk *et al.*, 1970; Thomson and Crawford, 1982). Their wavelength ($\approx$1000 km) and frequency (0.94–0.98 f) are compatible with the first mode (barotropic) shelf waves on a sloping shelf of 200–300-km width (Mysak, 1980). Thomson and Crawford (1982) showed that such waves can be generated by the diurnal tide currents at latitudes poleward of 30N and in regions where the bathymetry of the continental margin is able to support these high-frequency shelf wave motions. For our observations, the waves appeared to be forced by the local winds and there is no evidence of forcing by the diurnal tide. Since the frequency of oscillation is exactly diurnal, we suspect, however, that both tidal and wind forcings contribute to the generation of the observed diurnal shelf waves.

The second event (*Event C*, June 1986) took place south of 30N. The drifters with large diurnal oscillations were close to each other and the diurnal currents oscillated in phase. The observed ellipticity of the current ellipse is consistent with freely-propagating internal waves at frequency a few percent above the inertial frequency. These super-inertial waves were shown to be generated by the local wind stress.

A major event (*Event B*) of large near-inertial currents was generated by a tropical storm which moved northwest over the southern CCS in September 1985. The intense background mesoscale circulation was shown to alter significantly the effective frequency of the observed oscillations. In particular, a strong mesoscale eddy red-shifted the frequency of the oscillations by as much as 0.07 cpd. Interactions with the mean flow can be responsible for the disparity in the oscillation amplitudes (see drifters 10 and 13). It is, therefore, expected that the mean circulation plays an important role in setting the horizontal scales of the near-inertial currents and the consequent decay and propagation of surface near-inertial energy into the deep ocean.

Two comments should be made before closing this discussion. First, no consistent blue shift of the inertial frequency was observed. If there exists blue shifting associated with the β-effect or the spectral characteristics of the wind forcing, it must be weak compared to the frequency variations imposed by the mean circulation vorticity. Second, the decay time scale of the oscillations (≈ 10 inertial periods) is rather long compared to the observations of near-inertial currents reported in the literature. The Lagrangian character of the current observations (the location of observation and the near-inertial motions are advected by the mean circulation) might explain this result, especially since most oscillations are subinertial (or inertial) and should stay longer in the mixed layer.

Acknowledgments. This study was supported by the Office of Naval Research under contract N00014-87-K-0005. I wish to thank P. Niiler for giving me the opportunity to work with the drifter data set and for many valuable comments. This work benefited from scientific discussions with D. Luther, J. Paduan and L. Shay. Suggestions by E. Kunze and the anonymous reviewers were found helpful in the revision of the original manuscript.

APPENDIX 1

Complex demodulation at a slowly-varying frequency

The filtering operation called complex demodulation is a weighted least-squares fit of circularly-polarized oscillating currents at a given frequency on the velocity observations, over a specified moving time interval. Consider the complex time series $\mathbf{u}(t) = u(t) + i\, v(t)$ where u and v are respectively the zonal and meridional components of velocity. Assume that $\mathbf{u}(t)$ represents a drifter velocity from which we want to extract the energy at the local inertial frequency $f(t)$.[4] Suppose that $f(t)$ is slowly varying in time so that free inertial currents are solution of

$$\frac{d}{dt}\mathbf{u}(t) = -2\pi i\, f(t)\, \mathbf{u}(t). \tag{A1}$$

The least-squares fit model of the free inertial oscillations on the velocity observations over a time interval of length $2T$ around t_o reads

$$\mathbf{u}(t) \approx \alpha\, e^{-2\pi i f^*(t^*,t)t} \tag{A2}$$

where

$$f^*(t^*, t) = \frac{1}{t}\int_{t^*}^{t} f(t')\, dt' \tag{A3}$$

and t^* is arbitrary. The solution (also called demodulated signal or current) correspond-

4. Here, all frequencies are taken positive. The anticlockwise sense of rotation of the inertial currents is expressed by the minus sign in Eqs. (A1) and (A2).

ing to the minimum weighted sum of squares of the errors is

$$\alpha(t_o) = \langle w(t)e^{2\pi i f^*(t^*,t)t}\,\mathbf{u}(t)\rangle \tag{A4}$$

where

$$\langle\,\rangle = \frac{1}{2T}\int_{t_o-T}^{t_o+T} dt \tag{A5}$$

and $w(t)$ is a normalized data window $\langle w(t)\rangle = 1$. The skill S is the ratio of the variance accounted for by the model to the total variance of the velocity observations

$$S(t_o) = \frac{|\langle w(t)e^{-2\pi i f^*(t^*,t)t}\,\mathbf{u}(t)\rangle|^2}{\langle w(t)|\mathbf{u}(t)|^2\rangle}. \tag{A6}$$

The technique yields good results when the components of the signal to be explored correspond to a spectral peak.

APPENDIX 2

Simultaneous demodulation at two frequencies

In the presence of two substantial spectral peaks at a priori known frequencies, we can generalize the technique developed in Appendix 1 to extract simultaneously the energy in both peaks. For our Lagrangian data set, this method is used to analyze the variabilities of the energy in the inertial and diurnal bands. The model is

$$\mathbf{u}(t) \approx \alpha\, e^{-2\pi i t} + \beta\, e^{-2\pi i f^*(t^*,t)t} \tag{A7}$$

where $f^*(t)$ is defined in (A3). The best fit yields

$$\begin{bmatrix}\alpha(t_o)\\ \beta(t_o)\end{bmatrix} = M^{-1}\delta \tag{A8}$$

where

$$\delta = \begin{bmatrix}\langle w(t)e^{2\pi i t}\,\mathbf{u}(t)\rangle\\ \langle w(t)e^{2\pi i f^* t}\,\mathbf{u}(t)\rangle\end{bmatrix} \tag{A9}$$

and

$$M = \begin{bmatrix} 1 & \langle w(t)e^{-2\pi i(f^*-1)t}\,\mathbf{u}(t)\rangle\\ \langle w(t)\,e^{2\pi i(f^*-1)t}\,\mathbf{u}(t)\rangle & 1\end{bmatrix}. \tag{A10}$$

The skill for this two-oscillation fit is

$$S(t_o) = \frac{\delta^* M^{-1}\delta}{\langle w(t)|\mathbf{u}(t)|^2\rangle}. \tag{A11}$$

APPENDIX 3

The tidal ellipse

Any periodic motion at a given frequency f (1 cpd in our case) can be written as the sum of two circular oscillations rotating in opposite sense

$$\mathbf{u}(t) = u(t) + iv(t) = Ae^{2\pi ift} + Be^{-2\pi ift}, \tag{A12}$$

where $A = |A|e^{i\alpha}$ and $B = |B|\, e^{i\beta}$ are complex amplitudes. The velocity vector traces an ellipse whose major and minor axes have lengths $M = 2(|A| + |B|)$ and $m = 2(|B| - |A|)$ respectively. The inclination of the major axis with respect to the zonal direction is $\theta = \frac{1}{2}(\alpha + \beta)$. The sense of rotation of the velocity vector is anticlockwise if $m < 0$ and clockwise if $m > 0$.

In order to extract the energy at the diurnal frequency and to obtain the characteristics of the current ellipse, the two-oscillation model (A12) is least-squares fitted to the velocity observations. The complex coefficients A and B and the skill are computed using formulas similar to (A8)-(A11) and M, m and θ are easily estimated.

REFERENCES

Cartwright, D. E. 1969. Extraordinary tidal currents near St. Kilda. Nature, *223*, 928–932.

Craig, P. D. 1989. A model of diurnally forced vertical current structure near 30° latitude. Continental Shelf Res., *9*, 965–980.

D'Asaro, E. A. 1985. Upper ocean temperature structure, inertial currents, and Richardson numbers observed during strong meteorological forcing. J. Phys. Oceanogr., *15*, 943–962.

—— 1989. The decay of wind-forced mixed layer inertial oscillations due to the β-effect. J. Geophys. Res., *94*, 2045–2056.

FNWC. 1975. U.S. Naval Weather Service Numerical Environmental Products Manual, NAVAIR 50–1G–522.

Fu, L. -L. 1981. Observations and models of inertial waves in the deep ocean. Rev. Geophys. Space Phys., *19*, 141–170.

Gonella, J. 1972. A rotary-component method for analyzing meteorological and oceanographic vector time series. Deep-Sea Res., *19*, 833–846.

Haury, L. R., P. -M. Poulain, A. W. Mantyla, E. L. Venrick and P. P. Niiler. 1986. FRONTS cruise, data report. SIO Ref. 86–23, Scripps Institution of Oceanography, University of California, San Diego.

Hayward, T. L., A. W. Mantyla and P. P. Niiler. 1987. Physical, chemical and biological data, Cruise SQ86, 15–22 March, 1986. SIO Ref. 87–17, Scripps Institution of Oceanography, University of California, San Diego.

Hendershott, M. C. 1973. Inertial oscillations of tidal period. Progr. Oceanogr., *6*, 1–27.

Knauss, J. A. 1962. Observations of internal waves of tidal period. J. Mar. Res., *20*, 111–118.

Kundu, P. K. and R. E. Thomson. 1985. Inertial oscillations due to a moving front. J. Phys. Oceanogr., *15*, 1076–1084.

Kunze, E. 1985. Near-inertial wave propagation in geostrophic shear. J. Phys. Oceanogr., *15*, 544–565.

Large, W. G. and S. Pond. 1981. Open ocean momentum flux measurements in moderate to strong winds. J. Phys. Oceanogr., *11*, 324–336.

Lynn, R. J., K. A. Bliss and L. E. Eber. 1982. Vertical and horizontal distributions of seasonal mean temperature, salinity, sigma-*t*, stability, dynamic height, oxygen and oxygen saturation in the California Current, 1950–1978. California Cooperative Oceanic Fisheries Investigations, Atlas, 30, xii pp and 513 charts.

McComas, C. H. and P. Müller. 1981. Time scales of resonant interactions among oceanic internal waves. J. Phys. Oceanogr., *11*, 139–147.

Molinari, R. and A. D. Kirwan, Jr. 1975. Calculations of differential kinematic properties from Lagrangian observations in the western Caribbean Sea. J. Phys. Oceanogr., *5*, 483–491.

Munk, W. H. 1980. Internal wave spectra at the buoyant and inertial frequencies. J. Phys. Oceanogr., *10*, 1718–1728.

Munk, W. H. and N. Phillips. 1968. Coherence and band structure of inertial motion in the sea. Rev. Geophys. Space Phys., *6*, 447–472.

Munk, W. H., F. Snodgrass and M. Wimbush. 1970. Tides off-shore: Transition from California to deep-sea waters. Geophys. Fluid Dyn., *1*, 161–235.

Mysak, L. A. 1980. Recent advances in shelf wave dynamics. Rev. Geophys. Space Phys., *18*, 211–241.

Niiler, P. P., R. E. Davis and H. J. White. 1987. Water-following characteristics of a mixed layer drifter. Deep-Sea Res., *34*, 1867–1882.

Niiler, P. P., P. -M. Poulain and L. R. Haury. 1989. Synoptic three-dimensional circulation in an onshore-flowing filament of the California Current. Deep-Sea Res., *36*, 385–405.

Pazan, S. E., T. P. Barnett and A. M. Tubbs. 1982. Comparison of observed and model wind velocities. J. Appl. Meteor., *21*, 314–320.

Pollard, R. T. 1980. Properties of near-surface inertial oscillations. J. Phys. Oceanogr., *10*, 385–398.

Pollard, R. T. and R. C. Millard, Jr. 1970. Comparisons between observed and simulated wind-generated inertial oscillations. Deep-Sea Res., *17*, 813–821.

Poulain, P. -M. 1989. Surface circulation phenomena off Baja California as deduced from satellite-tracked drifters. Ph.D. dissertation, Scripps Institution of Oceanography, 124 pp.

Poulain, P. -M., J. D. Illeman and P. P. Niiler. 1987. Drifter observations in the California Current System (1985–1986), data report, SIO Ref. 87-27, Scripps Institution of Oceanography, University of California, San Diego.

Poulain, P. -M. and P. P. Niiler. 1989. Statistical analysis of the surface circulation in the California Current System using satellite-tracked drifters. J. Phys. Oceanogr., *19*, 1588–1603.

Prinsenberg, S.J., W. Willmot and M. Rattray, Jr. 1974. Generation and dissipation of coastal internal tides. Deep-Sea Res., *21*, 263–281.

Reid, J. L. 1962. Observations of inertial rotation and internal waves. Deep-Sea Res., *9*, 283–289.

Tennekes, H. and J. L. Lumley. 1987. A first Course in Turbulence, The MIT Press, 300 pp.

Thomson, R. E. 1983. A comparison between computed and measured oceanic winds near the British Columbia Coast. J. Geophys. Res. *88*, 2675–2683.

Thomson, R. E. and W. R. Crawford. 1982. The generation of diurnal period shelf waves by tidal currents. J. Phys. Oceanogr., *12*, 635–643.

Tukey, J. W. 1961. Discussion, emphasizing the connection between analysis of variance and spectrum analysis. Technometrics, *3*, 191–219 [also in The Collected Works of John W. Tukey, Volume I: Time series, 1949–1964, Wadsworth Publishing Company, Belmont, California, 650 pp, 1984].

Webster, F. 1968. Observations of inertial-period motions in the deep sea. Rev. Geophys., *6*, 473–490.

Weller, R. A. 1982. The relation of near-inertial motions observed in the mixed layer during the JASIN (1978) Experiment to the local wind stress and to the quasi-geostrophic flow field. J. Phys. Oceanogr., *12*, 1122–1136.
—— 1985. Near-surface velocity variability at inertial and subinertial frequencies in the vicinity of the California Current. J. Phys. Oceanogr., *15*, 372–385.

Received: *8 January, 1990;* revised: *13 August, 1990.*